

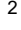




# Understanding the Effect of Grown-in Defects in Silicon on Solar Cell Efficiency

Jinta Mathew <sup>1</sup> , Bulent Arıkan <sup>2</sup> , Sercan Aslan <sup>2</sup> , Ryan Bugeja <sup>1</sup> , Davide La Fata <sup>1</sup> , Jessica Magro <sup>1</sup> , Vahdet Özyahni <sup>2</sup> , Selin Seyrek <sup>2</sup> , Nurhayat Yildirim <sup>3</sup> , Daniele Zingariello <sup>1</sup> , Marija Demicoli <sup>1,\*</sup> , Raşit Turan <sup>2</sup> , and Luciano Mule' Stagno <sup>1</sup> 

<sup>1</sup>Institute for Sustainable Energy - University of Malta, Malta

<sup>2</sup>Middle East Technical University - Center for Solar Energy Research and Applications (ODTÜ-GÜNAM), Turkey

<sup>3</sup>Kalyon PV Research and Development Center, Turkey

\*Correspondence: [marija.demicoli@um.edu.mt](mailto:marija.demicoli@um.edu.mt)

**Abstract.** Improving the efficiency of silicon-based solar cells is imperative to maximise harnessing of solar power. The current improvements in efficiency were attained by better manufacturing techniques and purer materials. There is however indirect evidence that the so-called agglomerated grown-in defects in silicon have a direct impact on cell efficiency and if this is the case, the efficiency could be improved by crystal engineering. This study focuses on understanding the defect generation and growth mechanisms in commercial silicon crystals and their impact on cell efficiency. Silicon wafers from different parts of the crystal having a range of oxygen and dopant concentrations and growth profiles, were investigated. These crystals were characterized using various tools and techniques such as Infrared Light Scattering Tomography (LST) to measure the defect density, and Fourier Transform Infrared Spectroscopy (FTIR) to measure the oxygen concentration. Solar cells were then fabricated out of these wafers to measure the performance of the devices. An understanding of why and how such defects impact the yield of different silicon wafers will lead to a thorough understanding of the relationship between the defect types, size and densities and cell efficiency. Moreover, this study will also shed light on the development of crystal recipes or after-crystal procedures to eliminate or minimize these effects on solar cell performance.

**Keywords:** Silicon Solar Cell, Defect Density, Light Scattering Tomography (LST), Efficiency, Fill Factor (FF).

## 1. Introduction

Czochralski (Cz)-grown silicon (Si) crystal accounts for most of the solar capacity installed worldwide [1], [2], [3]. The demand for silicon-based solar cells has grown tremendously in the past decade. The maximum theoretical efficiency of a single homojunction solar cell is about 30% [4]. Recent studies were able to obtain 27% efficiency [5], [6], which is attributable to the lesser defects in silicon. The efficiency of solar panels has increased over the years, with current improvements being attained by better manufacturing techniques and purer materials. The highest efficiencies are achieved on single-crystal Si by eliminating or reducing all losses, and by using the best and purest crystal substrate possible as other losses disappear, the effect of grown-in crystal defects on the efficiency of the solar cell is, in some cases, starting to be observed. A few published and privately communicated cases have confirmed over the last few years that grown-in defects, especially at the crystal extremities, can contribute to a reduction in efficiency for high-performance cells [7], [8], [9], [10]. During the Cz-Si ingot

growth, the target resistivity is achieved through the dopant concentration of the ingot. The dopant also has a direct effect on dopant-related bulk recombination and can also affect the dynamics of the recombination mechanism [7], [11], [12]. Apart from Doping, the location of a wafer along the ingot has a direct effect on the concentration of certain contaminants such as oxygen atoms from the quartz crucible. The crystal position also impacts the critical pull speed/thermal gradient ratio which directly affects the type and density of grown-in defects present [1]. Therefore, both base resistivity and the position of a wafer along the ingot have a direct relation with cell performance. It is crucial to study the influence of base resistivity and the position of the wafer on the efficiency of silicon solar cells. The focus of this work is thus to correlate the effect of these parameters with the efficiency of the solar cells.

The work presented in this paper will focus on understanding the defect generation and growth mechanisms in Si crystals, and on estimating their impact on the yield of high-end solar cells. Based on previous experience with semiconductor materials, this study started by specifically growing Cz-Si ingots with base resistivities of 0.2, 1.5 and ~650  $\Omega\cdot\text{cm}$  respectively at the KALYON PV facility. Si wafers from different sections along these ingots were investigated with the latter having a range of oxygen and dopant concentrations, as well as a potential range of grown-in defect densities. The material was then fully characterised using tools such as Fourier Transform Infrared imaging (FTIR) and Infrared Light Scattering Tomography (IR-LST). Such tools, in conjunction with the capability of fabricating solar cells, were used to precisely quantify the impact of the defect density on the cell efficiency. The results were analysed, and the solar cell yield of the different silicon wafers was compared, ultimately leading to the development of a preliminary correlation between defect density and solar cell efficiency.

## 2. Materials and Methods

The material samples used in this research were provided by the industrial partner, KALYON PV. In this study, 9N purity virgin polysilicon raw material was used for the mono-Si ingot production using the Cz method, with p-type ingots being produced by using boron dopant. During the crystal-growth process, high temperatures (1400-1500 °C) were used for the melting process while argon gas flow (70 L/min) was provided simultaneously to prevent the ingots from oxidation in the Cz furnaces. G1 size ingots were produced with 3-3.5 m length and 228 mm diameter. The crystal growth process is shown in Figure 1. Afterwards, all the produced ingots were firstly turned into bricks, then squared, and finally, 170  $\mu\text{m}$  wafers were produced by using a diamond wire saw to cut to G1 size (158.75 mm x 158.75 mm). All the produced wafers were analysed according to their electrical and geometrical parameters such as lifetime, resistivity, saw mark, total thickness variation (TTV) and microcracks by using HE-WI08, Hennecke Systems. Stemming from the fact that different parts of the silicon crystal can result in different oxygen amounts and growth profiles leading to different yields, thick samples from different locations within the ingot, ranging from seed-end (Section T) to tail-end (Section A), were obtained, as shown in Figure 2.

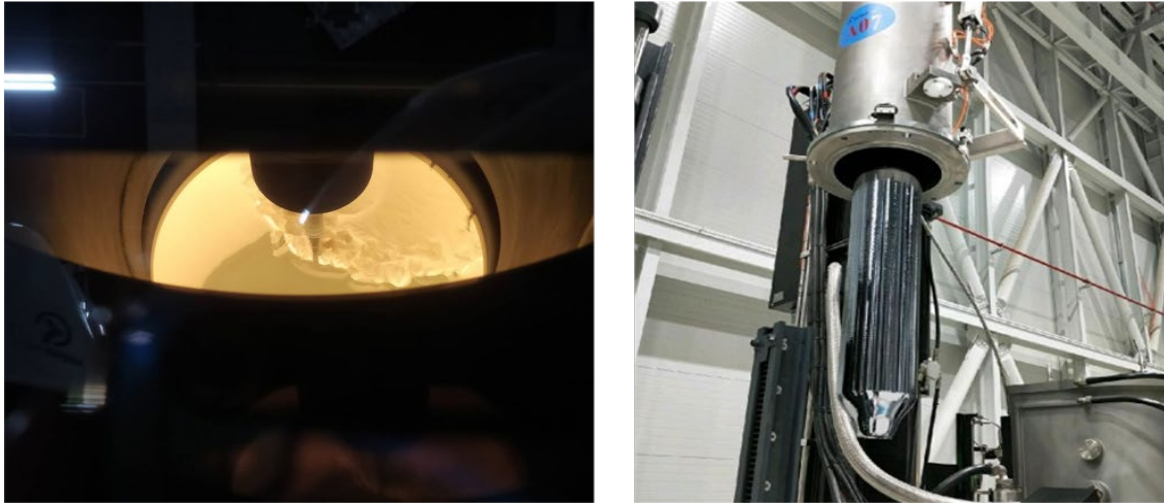


**Figure 1.** The crystal growth process at KALYON PV facility.

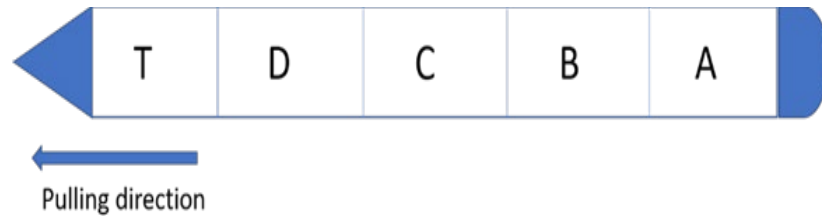


**Figure 2.** Silicon ingot locations are marked as T, D, C, B and A (from top to bottom). The arrow indicates the pulling direction. Section T refers to the seed-end while Section A refers to the tail-end.

Material characterisation techniques, such as LST and FTIR, require the material samples to have an optically specular surface to achieve optimum results. The silicon ingot slugs with a thickness of 0.7 - 1.5 mm were polished using the MultiPrep™ System, 8" polisher. Different abrasive papers were utilised for grinding, followed by the application of cloths that have a fine abrasive surface and a suitable liquid slurry to polish the samples up to a 0.05µm surface roughness. This procedure was followed to polish both the surface of the slug as well as the cleaved edge. Figure 3 shows the setup used for polishing the cleaved edge of the silicon slug.

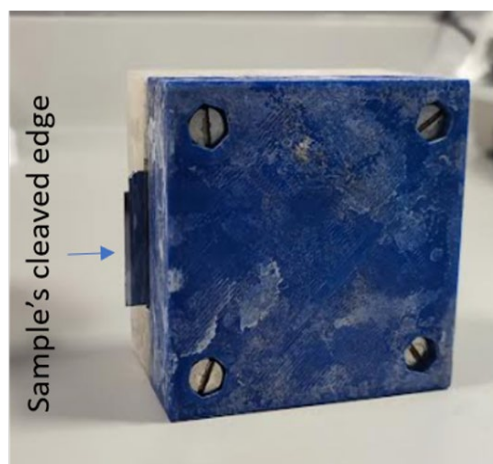


**Figure 3.** Setup used for polishing the cleaved edge of the silicon slug.

The polished samples were then examined using the LST tool from SEMILAB, whereby the sample is illuminated by IR light and the Rayleigh scattered light is collected to study the defects in the bulk of the samples. The laser scattering principle is used to obtain the characteristics from the bulk of the sample. The particle size and the light scattering are related,

and these are used to determine the density and size of the defects in the sample. If there are larger particles, the scattering angle is smaller, and the scattering intensity is higher. The concentration of oxygen in different locations of the silicon slug was also measured using FTIR (Bruker Vertex 80 FTIR Spectrometer).

Si wafers from adjoining crystal locations as the slugs used for LST and FTIR characterisation were simultaneously used for solar cell fabrication. The wafers were symmetrically textured in RENA BatchTex tool and the rear sides of the wafers were polished by using the masking approach in batch process. Phosphorus-doped emitters with sheet resistance of around  $95 \pm 5 \Omega/\square$  were formed by phosphorus oxychloride ( $\text{POCl}_3$ ) diffusion on both surfaces. Front and rear passivation layers, as well as anti-reflective coatings (ARCs), were deposited after single-side etching on the rear side. After the metallisation and firing steps, the I-V parameters of the produced Passivated Emitter and Rear Contact (PERC) solar cells were measured. Figure 4 shows a flowchart of this fabrication process.

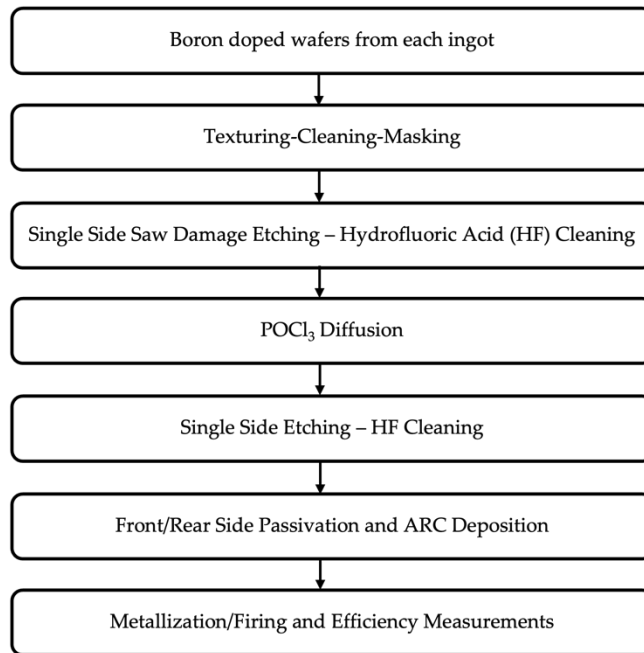


Figure 4. Flowchart depicting the solar cell fabrication process.

### 3. Results

This section will present the results of the characterization of the silicon samples using the LST and FTIR tools, as well as the performance measurements of the fabricated solar cells.

#### 3.1. LST Results

Figure 5 shows the defect densities as obtained by LST for the samples from different ingot sections (refer to Figure 2) and from ingots with different base resistivities ( $0.2$ ,  $1.5$  and  $\sim 650 \Omega\cdot\text{cm}$  respectively). It can be observed that there is a slight decrease in defect density for the slugs with base resistivities of  $0.2 \Omega\cdot\text{cm}$  (green) and  $1.5 \Omega\cdot\text{cm}$  (orange), and a more prominent decrease in defect density for slugs with base resistivity  $\sim 650 \Omega\cdot\text{cm}$  (red) as one moves from Section A (tail-end) to Section T (seed-end) of the ingot. In the case of the silicon ingot with resistivity  $\sim 650 \Omega\cdot\text{cm}$ , the mean defect density varies from  $2.2 \times 10^7$  to  $4.5 \times 10^6 \text{ cm}^{-3}$  as one moves from Section from A to Section T of the ingot (Figure 5(b)). For the silicon ingot with resistivity  $1.5 \Omega\cdot\text{cm}$ , the mean density of defects from Sections A, B, C, D, and T ranges from  $1.8 \times 10^7$  to  $1.1 \times 10^7 \text{ cm}^{-3}$  respectively (Figure 5(d)). Lastly, for the silicon ingot with resistivity  $0.2 \Omega\cdot\text{cm}$ , the defect density distribution ranges from  $1.45 \times 10^7$  to  $7.13 \times 10^6 \text{ cm}^{-3}$  from Section A to Section T of the ingot respectively (Figure 5(f)). These results show that Section T (seed-

end) has the lowest number of defects for all three ingots. It can therefore be concluded that while some variation in defect density has been observed within each crystal, there is no significant difference between the three crystals with different base resistivities.

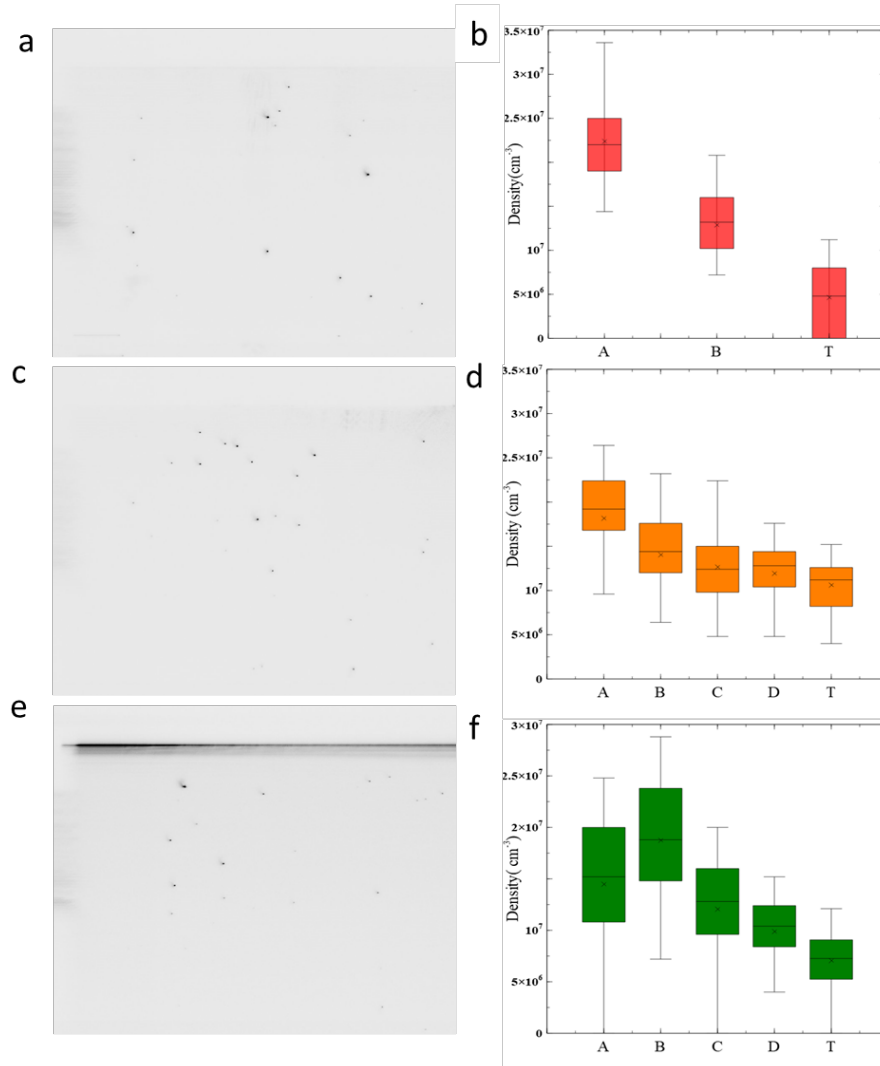


**Figure 5.** (a) and (b) LST image and defect density distribution of silicon samples with resistivity  $\sim 650 \Omega \cdot \text{cm}$  (red); (c) and (d) LST image and defect density distribution of silicon samples with resistivity  $1.5 \Omega \cdot \text{cm}$  (orange); (e) and (f) LST image and defect density distribution of silicon samples with resistivity  $0.2 \Omega \cdot \text{cm}$  (green). The defect density distribution is shown across different parts of the ingot – Sections A (tail-end), B, C, D and T (seed-end). The black dots in (a), (c) and (e) indicate the presence of defects while the cross symbols in (b), (d) and (f) mark the mean defect densities.

### 3.2 FTIR Results

The presence of oxygen within the ingot can create defects such as clusters of several oxygen atoms as well as  $\text{SiO}_2$  precipitates of various sizes and crystal structures [13], [14], [15], [16]. It can also result in vacancy-oxygen complexes which may then stabilise and grow in the crystal cooling phase. The oxygen measurement was done by FTIR and the results do not give any evidence of location-oriented dependence of oxygen in the ingot, as shown in Figure 6. FTIR measurements have shown that the amount of interstitial oxygen concentrations for wafers with base resistivities  $0.2 \Omega \cdot \text{cm}$ ,  $1.5 \Omega \cdot \text{cm}$  and  $\sim 650 \Omega \cdot \text{cm}$  were found to be between  $2.8$  to  $11.9 \times 10^{17}$  atoms/ $\text{cm}^3$ ,  $4.6$  to  $6.6 \times 10^{17}$  atoms/ $\text{cm}^3$ , and  $6.1$  to  $6.5 \times 10^{17}$  atoms/ $\text{cm}^3$  respectively.

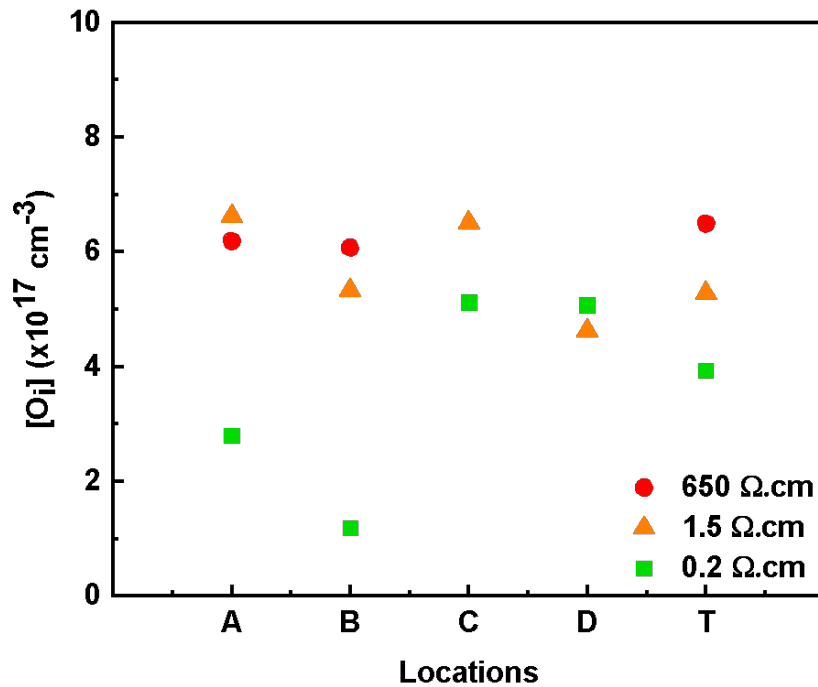


Figure 6. The oxygen concentration of the three silicon ingots as obtained by FTIR spectroscopy.

### 3.3 Solar cell results

The vital parameters of solar cell performance are open circuit voltage ( $V_{oc}$ ), short circuit current ( $I_{sc}$ ), Fill Factor (FF) and efficiency. Figure 7 shows the average I-V measurement result for at least eight PERC solar cells produced for each base resistivity. Figure 7(a) shows the open circuit voltage from different locations of the ingot. The dominant bulk effect can be seen in the  $V_{oc}$  results. The biggest  $V_{oc}$  obtained is from the undoped silicon wafers with base resistivity  $\sim 650 \Omega \cdot \text{cm}$ . The utmost open circuit voltage in the undoped solar cell may be the result of less impurity and the existence of fewer recombination centres in contrast with the medium-doped and heavily-doped solar cells with resistivities  $0.2 \Omega \cdot \text{cm}$  (green) and  $1.5 \Omega \cdot \text{cm}$  (orange) respectively. The heavily-doped or the lowest base resistivity solar cells have the lowest  $V_{oc}$  revealing that doping largely can induce more recombination centres. Doping alters the band structure of the crystalline silicon. This means that the value of open circuit voltage also depends on the bandgap of the silicon, and  $V_{oc}$ , in fact, increases with the increase of bandgap [17]. In contrast, the short circuit current value goes down when the bandgap increases, as is visible in the short circuit graph (Figure 7(b)). The lowest short circuit current is acquired from the solar cell with the highest resistivity of  $\sim 650 \Omega \cdot \text{cm}$ . The dependence of the FF on the location of the silicon ingots is illustrated in Figure 7(c). The determination of the FF is mainly based on the series resistance and the shunt resistance. The low FF of the undoped/high resistivity cells is a consequence of the high series resistance due to the larger base resistivity[18] Also, considering the FF of the medium and heavily doped silicon cell, the latter one has a slightly higher FF. Even so, the solar cells with a resistivity of  $1.5 \Omega \cdot \text{cm}$  (orange) have a FF of about 0.08, which is close to the heavily doped silicon cells (green).

The efficiency of the differently doped silicon solar cells along various positions of the ingot is shown in Figure 7(d). The doped crystals achieved efficiencies in the 20-21% range with the highest efficiency of 21.17% measured in the  $1.5 \Omega \cdot \text{cm}$  crystal. The lower efficiency in the undoped crystal is due to the absence of doping which results in lower charge carriers. Moreover, different regions of the same ingot have different efficiency values, with the

top/seed-end (Section T) of the silicon ingots with resistivities of 0.2  $\Omega$ .cm (green) and 1.5  $\Omega$ .cm (orange) having a better efficiency than other parts of the ingot. This indicates the possibility of the accumulation of more defects in some parts of the ingot such as the bottom part.

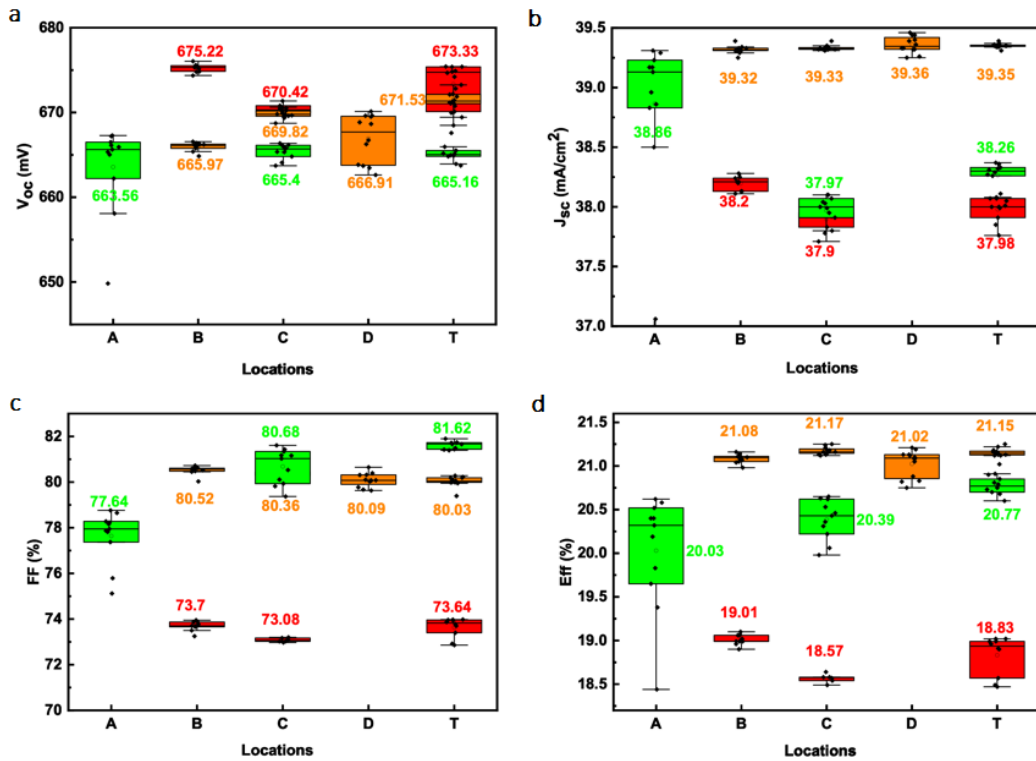


**Figure 7.** I-V measurement result for at least 8 PERC solar cells produced for each base resistivity. (a) Open circuit voltage; (b) Short circuit current; (c) Fill Factor; and (d) Efficiency along the locations A, B, C, D and T of the silicon ingot. Silicon ingots with resistivity 0.2  $\Omega$ .cm, 1.5  $\Omega$ .cm and ~650  $\Omega$ .cm are given by green, orange, and red colours respectively.

## 4. Discussion

This research paper focuses on the investigation of grown-in defects, defect generation and defect growth mechanisms in commercial Si crystals, and the effects of such defects on the yield of high-end solar cells. The results obtained from LST clearly show that the top part of the silicon ingots has a slightly smaller defect density than the other parts. The growth process is the main factor which affects the variation of defects across different locations of the same ingot. The combined analysis of the LST and solar cell results provides insights into obtaining a better solar cell efficiency from wafers located at the top and middle parts of the ingot. The accumulation of defects in the bottom part creates the probability of more recombination centres in these parts and the solar cells made from these sections have lower efficiency. Base resistivity plays a major role in the working of the solar cell. The higher base resistivity of 650  $\Omega$ .cm solar cell has the lowest efficiency which is due to the smaller number of charge carriers in the undoped silicon crystal. Silicon solar cells fabricated from wafers with a resistivity of 1.5  $\Omega$ .cm (medium doped) have the highest efficiency due to a greater number of charge carriers when compared to solar cells fabricated from wafers with a resistivity of 650  $\Omega$ .cm, as well as due to less recombination when compared to the cells made of silicon with a resistivity of 0.2  $\Omega$ .cm. Apart from the resistivity, there are other factors which can result in differences in the efficiency of the solar cell, though our study here focused more on the effects of grown-in defects and resistivity.



LST results have shown an apparent correlation with solar cell efficiency in the sense that LST-measured defect density seems to show an inverse relation with solar cell efficiency. One must caution however that the observed differences in efficiency were small, as were the differences in LST-measured defect densities obtained. Moreover, the LST has a defect detection limit of about 15nm [19], [20] which means that it could only be detecting part of the defect distribution, whereas presumably, any defect present will have an impact on solar cell efficiency. In this investigation, a slightly higher efficiency in the seed-end part of the crystal was observed. The dynamics of the crystal growth and the thermal profile to which the crystal sections are subjected influence the level of vacancies and subsequently, the agglomerated defect density. The seed-end part of the crystal tends to cool faster than the body since it has no other hot crystal material on top of it (which is the case for the rest of the body). The density and size of defects are also highly dependent on the oxygen concentration. Generally, high oxygen concentration typically results in smaller, but higher concentrations of vacancy-oxygen (V-O) defects. In this case, the oxygen concentration was kept well in control and there was no significant difference in the oxygen level between different sections. The tail-end section also cools faster at critical nucleation temperatures during crystal growth since after the body, a tail is grown where the pull rate is increased. This can result in a higher concentration of V-O defects in the bottom part of the crystal. In this particular study, while there is an apparent correlation of defect densities and efficiency along the crystal, the signals are too weak to reach further conclusions at this point. A more pronounced difference in defect concentration at the crystal extremities could have resulted in a stronger signal.

## 5. Conclusions

The main results presented in this work have compared the LST-measured defect density with solar cell efficiency for crystals with different base resistivities. Although the observed differences were small, they have shown an apparent correlation between defect density and efficiency in different parts of the crystal. In the three crystals grown, the oxygen level was stable and this did not result in the often-reported sharp drop in efficiency at the seed- or tail-end. The solar cells which are well-balanced between the number of charge carriers and the recombination rate can achieve good efficiency. Poor doping level leads to a reduced recombination rate but these solar cells undergo difficulties in attaining higher efficiency because of the fewer charge carriers. On the other hand, high doping creates a large number of charge carriers but the performance of the cell is affected by the higher recombination rate. It is necessary to have appropriate doping concentration to balance both factors to produce an efficient solar cell.

## Data Availability Statement

The data presented in this study are available on request from the corresponding author.

## Author Contributions

Conceptualization, L.M.S.; methodology, M.D., L.M.S. and R.T.; validation, J.Mathew, S.A., M.D., L.M.S. and R.T.; formal analysis, J.Mathew, S.A., M.D., L.M.S. and R.T.; investigation, J.Mathew, S.A., S.S., V.O., B.A., D.Z., R.B., J.M. and D.L.F.; resources, N.Y.; data curation, J.Mathew, S.A.; writing—original draft preparation, J.Mathew, S.A., M.D., L.M.S., N.Y.; writing—review and editing, J.Mathew, S.A., S.S., V.O., B.A., N.Y., D.Z., R.B., D.L.F., M.D., L.M.S., R.T.; visualization, J.Mathew, S.A.; supervision, M.D., L.M.S., and R.T.; project administration, M.D., L.M.S., and R.T; funding acquisition, M.D., L.M.S., and R.T. All authors have read and agreed to the published version of the manuscript.

## Conflicts of Interest

The authors declare no conflict of interest.



## Funding

This research was funded by the Energy and Water Agency (Malta) under the National Strategy for Research and Innovation in Energy and Water (2021-2030).

## Acknowledgements

The authors would like to acknowledge the support of Mr Paul Bonnici as lab officer within the Solar Research Laboratory at the Institute for Sustainable Energy at the University of Malta.

## References

- [1] J. Knobloch, S. W. Glunz, D. Biro, W. Warta, E. Schaffer, and W. Wettling, "Solar cells with efficiencies above 21% processed from Czochralski grown silicon," Conference Record of the IEEE Photovoltaic Specialists Conference, pp. 405–408, 1996, doi: 10.1109/PVSC.1996.564029.
- [2] X. Yu and D. Yang, "Growth of crystalline silicon for solar cells: Czochralski si," Handbook of Photovoltaic Silicon, pp. 129–174, Jan. 2019, doi: 10.1007/978-3-662-56472-1\_12.
- [3] X. Zhang et al., "Mass production of crystalline silicon solar cells with polysilicon-based passivating contacts: An industrial perspective," Progress in Photovoltaics: Research and Applications, vol. 31, no. 4, pp. 369–379, Apr. 2023, doi: 10.1002/PIP.3618.
- [4] W. Shockley and H. J. Queisser, "Detailed Balance Limit of Efficiency of p-n Junction Solar Cells," J Appl Phys, vol. 32, no. 3, pp. 510–519, Mar. 1961, doi: 10.1063/1.1736034.
- [5] W. Shen, Y. Zhao, and F. Liu, "Highlights of mainstream solar cell efficiencies in 2023," Frontiers in Energy, pp. 1–8, Feb. 2024, doi: 10.1007/S11708-024-0937-5.
- [6] A. Richter et al., "Design rules for high-efficiency both-sides-contacted silicon solar cells with balanced charge carrier transport and recombination losses," Nature Energy 2021 6:4, vol. 6, no. 4, pp. 429–438, Apr. 2021, doi: 10.1038/s41560-021-00805-w.
- [7] R. Falster, V. V. Voronkov, J. C. Holzer, S. Markgraf, S. McQuaid, and L. Mule' Stagno, "Intrinsic point defects and reactions in the growth of large silicon crystals," p. 1638, 1998, Accessed: Jan. 08, 2024. [Online]. Available: <https://www.um.edu.mt/library/oar/handle/123456789/110811>
- [8] F. Korsós et al., "Efficiency limiting crystal defects in monocrystalline silicon and their characterization in production," Solar Energy Materials and Solar Cells, vol. 186, pp. 217–226, Nov. 2018, doi: 10.1016/J.SOLMAT.2018.06.030.
- [9] L. Chen et al., "Effect of oxygen precipitation on the performance of Czochralski silicon solar cells," Solar Energy Materials and Solar Cells, vol. 95, no. 11, pp. 3148–3151, Nov. 2011, doi: 10.1016/J.SOLMAT.2011.06.044.
- [10] B. Lim, K. Bothe, and J. Schmidt, "Impact of oxygen on the permanent deactivation of boron-oxygen-related recombination centers in crystalline silicon," J Appl Phys, vol. 107, no. 12, Jun. 2010, doi: 10.1063/1.3431359.
- [11] Q. Wang et al., "Impact of boron doping on electrical performance and efficiency of n-TOPCon solar cell," Solar Energy, vol. 227, pp. 273–291, Oct. 2021, doi: 10.1016/J.SOLENER.2021.08.075.

- [12] V. A. Trukhanov, V. V. Bruevich, and D. Y. Paraschuk, "Effect of doping on performance of organic solar cells," *Phys Rev B Condens Matter Mater Phys*, vol. 84, no. 20, p. 205318, Nov. 2011, doi: 10.1103/PHYSREVB.84.205318/FIGURES/21/MEDIUM.
- [13] A. Borghesi, B. Pivac, A. Sassella, and A. Stella, "Oxygen precipitation in silicon," *J Appl Phys*, vol. 77, no. 9, pp. 4169–4244, May 1995, doi: 10.1063/1.359479.
- [14] W. Bergholz, "Chapter 12 Grown-in and Process-Induced Defects," *Semiconductors and Semimetals*, vol. 42, no. C, pp. 513–575, Jan. 1994, doi: 10.1016/S0080-8784(08)60255-0.
- [15] L. Chen et al., "Effect of oxygen precipitation on the performance of Czochralski silicon solar cells," *Solar Energy Materials and Solar Cells*, vol. 95, no. 11, pp. 3148–3151, Nov. 2011, doi: 10.1016/J.SOLMAT.2011.06.044.
- [16] R. Kvande, Ø. Mjøs, and B. Rynningen, "Growth rate and impurity distribution in multicrystalline silicon for solar cells," *Materials Science and Engineering: A*, vol. 413–414, pp. 545–549, Dec. 2005, doi: 10.1016/J.MSEA.2005.09.035.
- [17] H. T. Nguyen and D. Macdonald, "On the composition of luminescence spectra from heavily doped p-type silicon under low and high excitation," *J Lumin*, vol. 181, pp. 223–229, Jan. 2017, doi: 10.1016/j.jlumin.2016.08.036.
- [18] D. Macdonald and A. Cuevas, "Reduced Fill Factors in Multicrystalline Silicon Solar Cells Due to Injection! level Dependent Bulk Recombination Lifetimes," 1999, doi: 10.1002/1099-159X(200007/08)8:4<363::AID-PIP328>3.0.CO;2-Y.
- [19] J. Ellis, S. Heinemeyer, K. A. Olive, G. Weiglein, "Phenomenological indications of the scale of supersymmetry". *Journal of High Energy Physics*. vol. 2006. JHEP05(2006). doi: 10.1088/1126-6708/2006/05/005
- [20] K. Sakai, "Detection limit for defect density by light scattering tomography," *Japanese Journal of Applied Physics, Part 1: Regular Papers and Short Notes and Review Papers*, vol. 45, no. 9 A, pp. 7181–7183, Sep. 2006, doi: 10.1143/JJAP.45.7181.